J Mater Sci (2008) 43:4483–4486
DOI 10.1007/s10853-008-2652-8

Adiabatic shear failure of high reinforcement content aluminum matrix composites

G. H. Wu · D. Z. Zhu · G. Q. Chen · L. T. Jiang · Q. Zhang

Received: 19 January 2008 / Accepted: 11 April 2008 / Published online: 29 April 2008

Abstract Dynamic failure behaviors of high reinforcement content TiB_2/Al composites were experimentally investigated using split Hopkinson pressure bar (SHPB). The TiB_2/Al composites showed high flow stresses and good plastic deformation ability at high strain rates. Adiabatic temperature rise decreased the flow stresses of TiB_2/Al composites, which was verified by the prediction of Johnson–Cook model. While the predictions by Cowper–Symonds model exhibited obvious strain hardening characteristic, the values of which were much higher than those of the Johnson–Cook model and the experimental. The composites were failed macroscopically in brittle fracture and some phase transformation bands were found on the shearing surfaces. The dynamic failure behavior of TiB_2/Al composites was predominated by the formation of adiabatic shear bands.

Introduction

The formation of adiabatic shear band (ASB) has been confirmed as a major mechanism for dynamic failure in metallic materials as Fe, Ti, and Al. Most of the researches have primarily concerned with the critical conditions leading to ASB initiation and the microstructure of shear bands including deformed bands and transformed bands [1–3]. Occurring of deformed ASB has also been found in aluminum matrix composites (AMC), especially for those with low reinforcement content ($\sim$25 vol.%). Ling [4] demonstrated that the formation of ASB in the SiC/2124Al composites reinforced with smaller particles was more readily observed than that reinforced with larger particles. Owolabi et al. [5] and Dai [6, 7] confirmed that the susceptibility of aluminum alloy to strain localization and adiabatic shear failure increased with particulate reinforcement. They concluded that the higher the particle content, the higher the strain gradient. That is, the high reinforcement content composites are prone to adiabatic shear localization. However, little information has been reported on the adiabatic shear failure of high reinforcement content AMC.

High reinforcement content AMC reinforced with ceramic particles as SiC, Al_2O_3, and TiB_2 are candidate materials for lightweight armors and protective coatings as well as electronic packaging components [8, 9]. When used for these applications, dynamic failure behaviors of these materials are most important. Some researchers ascribed the dynamic failure of high reinforcement content AMC to the internal damage accumulation, not adiabatic shear localization [10–13]. Therefore, further studies on dynamic failure behaviors of high reinforcement content AMC are still essential. In this study, the dynamic compression properties of 55, 65 vol.%TiB_2/Al composites at 1410–1650 s^{-1} were measured using split Hopkinson pressure bar (SHPB). The microstructures of fracture specimens were characterized by scanning electron microscope (SEM), and the effects of adiabatic temperature rise on dynamic compressive properties were analyzed.

Materials and experimental methods

The materials used in this study are 2024 aluminum alloy reinforced with 55, 65 vol.% TiB_2 ceramic particulates. In

G. H. Wu · D. Z. Zhu (✉) · G. Q. Chen · L. T. Jiang · Q. Zhang
School of Materials Science and Engineering, Harbin Institute of Technology, P.O. 3023, Science Park, No. 2 Yikuang Street, Harbin, Heilongjiang 150080, People's Republic of China
e-mail: zdzandy@126.com

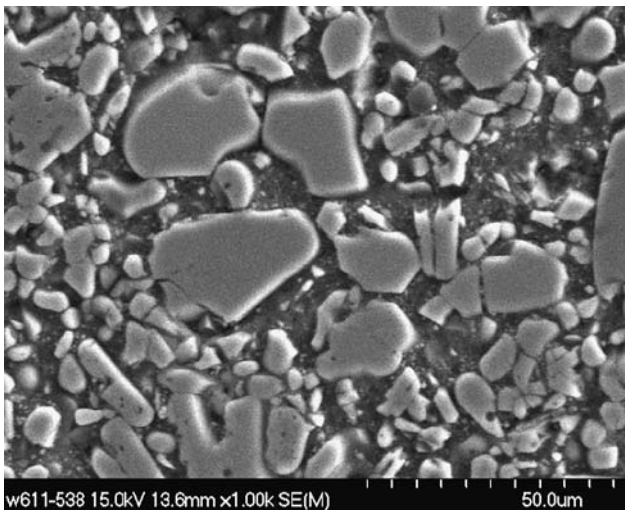

Fig. 1 Representative optical micrograph of TiB_2/2024Al composites

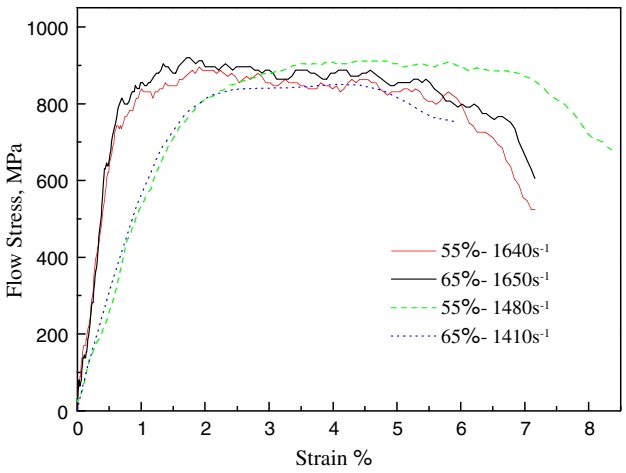

Fig. 2 Dynamic compressive stress–strain curves of TiB_2/Al composites

order to obtain a high reinforcement volume fraction, TiB_2 particles of 6 and 25 μm with a weight ratio of 5:1 were used. The TiB_2 particles preforms were prepared in air by tapping dry powder into the steel molds. The composites were fabricated by pressure infiltration method, including the infiltration of melted aluminum alloy into TiB_2 particles preforms and the solidification of the composites under pressure. Representative optical micrograph of TiB_2/2024Al composites is shown in Fig. 1. It can be seen that dual-sized particles are packed tightly by the particle–particle contacting within the composites. The continuity of aluminum matrix is weakened by reinforcement particles.

Before testing, T6 heat treatment was performed on TiB_2/Al composites. This involves a solid solution treatment at 768 K for 1 h followed by aging treatment at 433 K for 10 h. The materials were machined into cylindrical test specimens 8 mm in diameter and 16 mm in length. Direct impact SPHB was used to conduct high strain-rate compression tests on these specimens. The interfaces between the specimens and the compression platens were lubricated in order to reduce friction. All the compression specimens were observed using S-570 SEM.

Dynamic compression and adiabatic shearing

Figure 2 shows the typical stress–strain curves of 55 and 65% TiB_2/Al composites under dynamic loading. Compared to the compressive stress–strain curve at 1480 s^{-1}, the 55% TiB_2/Al composite at 1640 s^{-1} exhibits significant strain-rate hardening and thermal softening characteristic. The 65% TiB_2/Al composite shows the similar compression deformation behavior as the 55%. Additionally, it exhibits a higher compressive strength than the 55%. The 65% TiB_2/Al composite gets a peak flow stress as 913 MPa at 1.7% strain, which is 131 MPa higher than that at 1410 s^{-1} at the same strain (1.7% strain). After that, the flow stress softening phenomenon appears and the flow stress decreases by ~156 MPa till 6.7% strain. Subsequently, it drops sharply in the range 6.7–7.1% strain, which means a failure for the 65% composite.

The 55 and 65% TiB_2/Al composites are both failed macroscopically in shearing fracture and some white bright spots and groups are found on the fracture surfaces, shown in Fig. 3a. Figure 3b shows the phase transformation bands

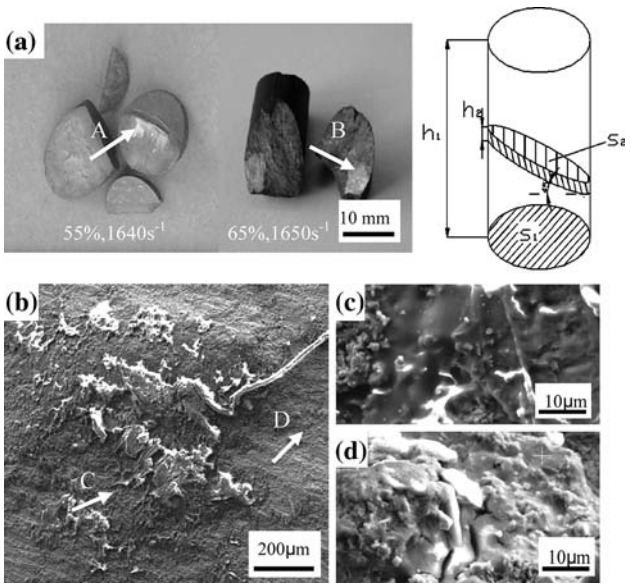

Fig. 3 Adiabatic shear failure for TiB_2/Al composites: (**a**) specimens failed in shearing and schematic diagram of adiabatic shear layer, (**b**) melted aluminum groups at 1650 s^{-1}, (**c**) magnified image in the margins of melted aluminum at point C, and (**d**) magnified image outside of the melted aluminum at point D

within the 65% TiB_2/Al composite at 1650 s^{-1}. The melted aluminum matrix is dispersed as branches and groups on the shearing surfaces, the diameter of which is in the range 50–300 μm. Some melted aluminum bands are also found in Fig. 3b with an average width of 20 μm, which are much narrower than that of deformed bands (~200 μm) for Al_2O_3/6061Al composites investigated by Owolabi et al. [5]. Figure 3c reveals that the reinforcement particles located in the margins of melted aluminum groups are surrounded by the melted aluminum matrix. Even the broken particles far from the melted aluminum bands, shown in Fig. 3d, are covered by a thin layer of melted aluminum. This implies that the adiabatic shear failure for TiB_2/Al composites was predominated by the melted/softened aluminum matrix.

The average adiabatic temperature rise for metallic materials as Al, Ti, and Fe can be calculated using a conventional formula as [1, 3, 10]:

$$\Delta T = \int_0^{\varepsilon_f} \frac{\beta\sigma}{\rho C_m} d\varepsilon \tag{1}$$

where β is the fraction of the plastic work converts into heat, ε_f is the final plastic strain, ρ is the density, and C_m is the specific heat for the matrix. An average temperature rise of ~5 K calculated by Eq. 1 has been reported for the 55% Al_2O_3/Al composites [13]. In the present study, the average temperature rise is in the range 15–20 K. Obviously, the deformed bands (commonly occurred at 0.4–0.5T_m) cannot occur in terms of the average temperature, even the phase transformation bands. Therefore, Eq. 1 is not suitable for describing the formation of ASBs within metal matrix composites.

In fact, high temperature is just existed in local regions for metals and inhomogeneous materials. The melting/softening phenomenon is also found in Zr-based bulk amorphous alloys containing tungsten [14]. The heat diffusion distance within the TiB_2/Al composites can be estimated as a formula: $L = 2\sqrt{\alpha t}$, and gets a value less than 0.35 mm. Thus, we suppose that all adiabatic heat is accumulated on the shear layer with a corner of 45° to the applied force axis, as shown in Fig. 3a. Local temperature rise for the shear layer is ΔT_1 and can be derived as:

$$\Delta T_1 = \frac{\beta}{\rho C_m} \frac{S_1 h_1}{S_2 h_2} \int_0^{\varepsilon_f} \sigma d\varepsilon \tag{2}$$

where $S_2 = S_1/\cos 45°$, $h_1 = 16$ mm, the thickness (h_2) of adiabatic shear layer (pointed as arrows A and B in Fig. 3a) is measured 0.05–0.18 mm from the specimen section where melted aluminum is located. The value of ΔT_1 is calculated higher than 980 K. Therefore, the phase transformation might take place at the 45° shear layer. However, local temperature rise is roughly estimated here and precise measurement should be conducted in our next work.

Modeling on stress–strain curves

In order to analyze the effect of adiabatic temperature rise on dynamic deformation behavior, Cowper–Symonds model [15] and Johnson–Cook model [16] are chosen in the present numerical analysis. An axisymmetric unit cell model is adopted and the cell aspect ratios A_p is assigned as 1 and 2 for considering the shapes of particles. More details on unit cell model can be found in the investigations of Bao and Lin [10] and Li and Ramesh [12]. The calculation software LS-DYNA is used to compute the overall response of the composites under uniaxial compression.

The Cowper–Symonds model is commonly used for monolithic metallic materials as steel and aluminum, and described as:

$$\sigma = \sigma_s \left[1 + \left(\frac{\dot{\varepsilon}}{D}\right)^{1/p}\right] \tag{3}$$

where σ is the dynamic flow stress at a uniaxial plastic strain rate $\dot{\varepsilon}$, σ_s is the associated static flow stress, the material constants D and p are given as 22515 s^{-1} and 4.84, respectively. The Johnson–Cook model is extensively used for metals, alloys, and ceramics. It describes the competition between thermal softening and the strain hardening and strain rate hardening comprehensively, and is expressed as:

$$\sigma = [A + B\varepsilon^n]\left[1 + C\ln\frac{\dot{\varepsilon}}{\dot{\varepsilon}_0}\right]\left[1 - \left(\frac{T - T_0}{T_m - T_0}\right)^m\right] \tag{4}$$

where T is the temperature within the unit cell and can be calculated by Eq. 1. T_m and T_0 are the melting temperature and the initial temperature, respectively. The dynamic mechanical properties of 2024Al-T6 were measured, and

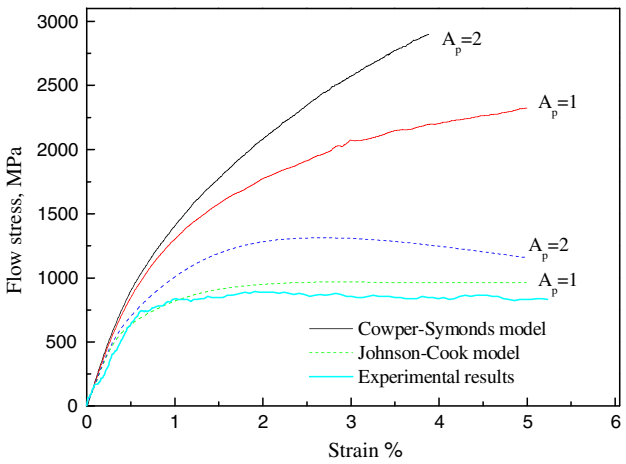

Fig. 4 Dynamic stress–strain curves predicted by the Cowper–Symonds model and Johnson–Cook model of 55% TiB_2/Al composite at 1640 s^{-1}

the coefficients A, B, C, m, and n [17] are given as: A = 345.4 MPa, B = 628.7 MPa, C = 0.0128, m = 1.5282, n = 0.73315. For the limitations of unit cell model, only the stress–strain curves of 55% TiB_2/Al composite are calculated, as shown in Fig. 4.

Figure 4 illustrates that the predictions by the Johnson–Cook model with A_p of 1 agree well with the experimental data. Although the flow stress predicted by the Johnson–Cook model with A_p of 2 is a bit higher than the experimental, it exhibits the similar flow softening characteristic as the experimental curve at 2–5% strain. While the stress–strain curves predicted by the Cowper–Symonds model exhibit obvious strain hardening characteristic, the values of which are much higher than those of the Johnson–Cook model and the experimental. This indicates that the local temperature rise within the composite is high enough to soften the flow stress at high strain rates.

Conclusions

In summary, the 55 and 65% TiB_2/Al composites are failed in adiabatic shearing at 1410–1650 s^{-1}. The dynamic failure for TiB_2/Al composites is caused by the growth and coalescence of melted aluminum bands, the diameter of which is in the range 50–300 μm. The predictions of the Johnson–Cook model agree well with the experimental values.

References

1. Wei Q, Kecskes L, Jiao T, Hartwig KT, Ramesh KT, Ma E (2004) Acta Mater 52:1859. doi:10.1016/j.actamat.2003.12.025
2. Rosakis AJ, Ravichandran G (2000) Int J Solids Struct 37:331. doi:10.1016/S0020-7683(99)00097-9
3. Wang XB (2006) Trans Nonferrous Met Soc China 16:333. doi:10.1016/S1003-6326(06)60057-5
4. Ling Z (2000) J Comp Mater 34:101. doi:10.1106/4ET5-AB4L-B6XT-TR08
5. Owolabi GM, Odeshi AG, Singh MNK, Bassim MN (2007) Mater Sci Eng A 457:114. doi:10.1016/j.msea.2006.12.034
6. Dai LH, Ling Z, Bai YL (1999) Scripta Mater 41:245. doi:10.1016/S1359-6462(99)00153-0
7. Dai LH, Liu LF, Bai YL (2004) Int J Solids Struct 41:5979. doi:10.1016/j.ijsolstr.2004.05.023
8. Zhang Q, Chen GQ, Wu GH, Xiu ZY, Luan BF (2003) Mater Lett 57:1453. doi:10.1016/S0167-577X(02)01006-6
9. Zhao M, Wu GH, Dou ZY, Jiang LT (2004) Mater Sci Eng A 374:303. doi:10.1016/j.msea.2004.03.003
10. Bao G, Lin Z (1996) Acta Mater 44:1011. doi:10.1016/1359-6454(95)00236-7
11. Li Y, Ramesh KT, Chin ESC (2000) Acta Mater. 48:1563. doi:10.1016/S1359-6454(99)00430-9
12. Li Y, Ramesh KT (1998) Acta Mater 46:5633. doi:10.1016/S1359-6454(98)00250-X
13. Marchi CS, Cao FH, Kouzeli M, Mortensen A (2002) Mater Sci Eng A 337:202. doi:10.1016/S0921-5093(02)00035-7
14. Hui XD, Kou HC, He JP, Wang YL, Dong W, Chen GL (2002) Intermetallics 10:1065. doi:10.1016/S0966-9795(02)00145-0
15. Symonds PS (1965) In: Huffington NJ (ed) Behavior of materials under impact loading. ASME, New York, p 106
16. Johnson GR, Cook WH (1985) Eng Fract Mech 21:31. doi:10.1016/0013-7944(85)90052-9
17. Meyers MA (1994) Dynamic behavior of materials. Wiley, New York, p 228